# OSCILLATIONS IN HIGH-ORDER FINITE DIFFERENCE SOLUTIONS OF STIFF PROBLEMS ON NON-UNIFORM GRIDS

ADRIAN S. SABAU AND PETER E. RAAD*

*Mechanical Engineering Department, Southern Methodist University, Dallas, TX 75275-0337, USA*

## SUMMARY

This work investigates the mitigation and elimination of scheme-related oscillations generated in compact and classical fourth-order finite difference solutions of stiff problems, represented here by the Burgers and Reynolds equations. The regions where severe gradients are anticipated are refined by the use of subdomains where the grid is distributed according to a geometric progression. It is observed that, for multi-domain solutions, both the classical and compact fourth-order finite difference schemes can exhibit spurious oscillations. When present, the oscillations are initially generated around the interface between the uniform and non-uniform grid subdomains. Based on a thorough study of the grid distribution effects, it is shown that the numerical oscillations are caused by inadequate geometric progression ratios within the non-uniformly discretized subdomains. Indeed, accurate solutions are obtainable if and only if the grid ratios in the non-uniform subdomains are greater than a critical threshold ratio. It is concluded that high-order classical and compact schemes can be used with confidence to efficiently solve one- or two-dimensional problems whose solutions exhibit sharp gradients in very thin regions, provided that the numerically generated oscillations are eliminated by an appropriate choice of grid distribution within the non-uniformly discretized subdomains. Copyright © 1999 John Wiley & Sons, Ltd.

KEY WORDS:   high-order finite difference schemes; oscillations; non-uniform grids; stiff problems

## 1. INTRODUCTION

In fluid dynamics, one is often faced with stiff problems whose solutions involve sharp variations in the dependent variable over very thin regions [1]. In order to numerically resolve these 'boundary or interior layers,' which can be as much as six orders of magnitude smaller than the overall length of the domain (see e.g. [2]), one must use a grid distribution refined commensurately with the gradients in those layers. It is imperative, however, to localize the finer grid resolutions to only those regions in order to avoid making the computational solution of such problems prohibitively expensive. The localization of grid refinement can be achieved by a combined use of multi-domains and non-uniform grid distributions. Another advantageous approach to maintaining computational efficiency is the use of higher-order methods, such as classical and compact fourth-order finite difference methods. These methods have been successfully used in fluid dynamics, but only for problems with moderate gradients over thin layers. In fact, it is widely held that when applied to stiff problems discretized with

non-uniform grid distributions, higher-order methods achieve much lower than expected accuracies [3,4], with scheme-related spurious oscillations limiting the use of what otherwise are highly efficient schemes. The goal of this work is, therefore, to investigate this important question regarding the suitability of classical and compact fourth-order FD methods for solving stiff problems on non-uniform, multi-domain grids. During this investigation it will also be possible to ascertain in detail the potential role played by the grid distribution in the elimination of scheme-related spurious oscillations, and to determine the existence of a minimum threshold value of the grid ratio used to geometrically refine those regions where severe gradients are anticipated. Knowledge of the threshold value, above which spurious oscillations are eliminated, makes it possible to achieve higher-order-accurate solutions with a minimal grid resolution.

Improvements in the solutions of boundary layer problems, such as the ones mentioned above can be obtained by the use of adaptive grid techniques [5,6] as well as by local grid refinement [3]. Additionally, oscillations can be dampened either by adding artificial viscosity to the original equations or by using dissipative schemes such as the upwind schemes [1]. However, as pointed out by Gresho and Lee [7], such dissipative techniques provide accurate solutions only when a fine grid is used, which guarantees that 'the numerical diffusion is significantly less than the physical diffusion'. Another approach is to use filtering algorithms as post-processors to the conventional techniques [8,9]. However, an effective approach for resolving the large gradients in boundary and interior layers is to refine the grid only in those layers without affecting the remainder of the computational domain.

In this paper, the grid refinement is achieved by allowing the grid to grow geometrically within the boundary or interior layer subdomains, while the remainder of the domain is discretized with a uniform spacing. The geometrically distributed grid is generated very efficiently and makes it possible to obtain accurate solutions for boundary layer problems. Fletcher [3] and Varghese and Raad [10] among many other researchers, indicate that it is preferable to distribute the grid points in the non-uniform subdomains with a ratio larger than a threshold value of 0.8. This assertion is motivated by the fact that as the grid ratios approach 1, the higher formal accuracy of FD schemes on a uniform grid is recovered.

High-order FD schemes and their applicability to problems in fluid dynamics have received much attention. Fornberg [11] provided an algorithm for generating high-order FD formulae on arbitrarily spaced grids. Hoffman and Reddy [12] studied high-order approximations formulae for functions and their derivatives by means of Chebyshev polynomial interpolation. Beam and Warming [13] and Lele [14] studied the dissipative and dispersive properties of high-order methods, but in the context of a uniform grid. Gartland [15] used high-order FD schemes on a uniform mesh to solve the model linear source problem $-(pu')' + qu = f$ where $p$, $q$, and $f$ can have jump discontinuities.

Compact FD schemes have been successfully applied to fluid dynamics problems with moderate gradients over a thin interior or boundary layer. Adam [16] proposed compact FD boundary formulations and improved the efficiency of compact schemes for the solution of Burgers equation. Rubin and Khosla [17] provided compact schemes on a non-uniform mesh by the use of spline interpolation. Aubert and Deville [18] applied compact schemes to a mapped domain for a Stokes flow problem with $Re \geq 100$.

In Section 2, a method based on the factored implicit scheme of Beam and Warming [13] for a class of conservative equations is presented along with an analysis of the effects of varying the defining grid parameters on the non-uniform grid distribution. Section 2.3 describes briefly the derivations of classical and compact FD schemes on a non-uniform mesh with application to a geometrically refined grid. The test problems are described in Section 3. In Section 4, it

is shown that numerical oscillations are generated at the interface between the uniform and non-uniform grid subdomains. The interface oscillations are shown to be due to an inadequate geometric growth ratio $r$ within the non-uniform grid subdomain. Based on a combined study of the effects of the grid parameters on the spurious oscillations, it is shown that the oscillations can be eliminated with a minimum of additional grid points (and therefore with minimal additional computational effort) by using geometric ratios whose values are greater than threshold values. Larger grid ratios are achieved by decreasing the value of the interface ratio or by increasing the width of the non-uniform subdomain rather than by decreasing the uniform grid spacing. Although decreasing the uniform grid spacing has traditionally been the main focus in obtaining more accurate solutions, it is a much less effective and prohibitively more expensive choice.

## 2. METHODOLOGY

### 2.1. Temporal approximation scheme

In this section, the development of a two-dimensional, implicit, FD method for non-linear conservative equations, based on the Beam and Warming [13] factored-implicit scheme, is presented, which is a general algorithm for solving equations that can be written in the conservative form:

$$\frac{\partial u}{\partial t} + \frac{\partial F(u)}{\partial x} + \frac{\partial G(u)}{\partial y} = \frac{\partial V_1(u, u_x)}{\partial x} + \frac{\partial V_2(u, u_y)}{\partial x} + \frac{\partial W_1(u, u_x)}{\partial y} + \frac{\partial W_2(u, u_y)}{\partial y}. \tag{1}$$

If the Beam and Warming [13] conservation law is used in conjunction with fourth-order-accurate spatial approximations, the first derivatives of the dependent variable must be computed beforehand at every time step with the same high-order of accuracy. The expensive computation of the first derivatives can be avoided by writing a conservation law equation in an alternative form, namely:

$$\frac{\partial u}{\partial t} = \frac{\partial F_1(u, h)}{\partial x} + \frac{\partial F_2(u, h)}{\partial y} + \frac{\partial^2 G_1(u, h)}{\partial x^2} + \frac{\partial^2 G_2(u, h)}{\partial y^2} + \frac{\partial^2 H(u, h)}{\partial x\,\partial y}, \tag{2}$$

which can be readily discretized with high-order FD schemes. Here $h(x, y, t)$ is a known function included for the sake of generality. Although Equation (1) cannot in general be rewritten as Equation (2), it must be emphasized that most equations that describe fluid dynamics phenomena can be cast in a conservative form similar to that given by Equation (2). For example, the $x$-component of the Navier–Stokes equations for a viscous compressible fluid can be written in the following conservative form:

$$\frac{\partial u^*}{\partial t} = \left(-\frac{1}{\rho} u^{*2}\right)_x + \left(-\frac{1}{\rho} u^* v^*\right)_y + \left(\frac{4v}{3} u^*\right)_{xx} + (vu^*)_{yy} + \left(\frac{v}{3} v^*\right)_{xy}, \tag{3}$$

where $\rho$, $u^* = \rho u$ and $v^* = \rho v$ are taken as primary variables instead of $\rho$, $u$ and $v$. As shown in Section 3, Burgers and Reynolds equations can also be written in conservative form given by Equation (2).

Various time differencing schemes were combined by Warming and Beam [19] into a general Padé form as follows:

$$\Delta u^k \equiv u^{k+1} - u^k$$

$$= \sigma_1 \frac{\partial}{\partial t}(\Delta u^k) + \sigma_2 \frac{\partial}{\partial t}(u^k) + \sigma_3 \Delta u^{k-1} + O\left[\left(\zeta - \frac{1}{2} - \eta\right)\Delta t^2 + \Delta t^3\right], \quad (4)$$

where superscripts $k-1$, $k$ and $k+1$ refer to the old, current and new time levels respectively; $\sigma_1$, $\sigma_2$ and $\sigma_3$ are constants defined as:

$$\sigma_1 = \frac{\zeta \Delta t}{1 + \eta}; \qquad \sigma_2 = \frac{\Delta t}{1 + \eta}; \qquad \sigma_3 = \frac{\eta}{1 + \eta}; \quad (5)$$

and $O[\ldots]$ refers to the order of magnitude of the temporal truncation error. For the 3-point backward time differencing scheme used throughout this work, $\zeta$ and $\eta$ are set equal to 1 and 0.5 respectively. Other time differencing formulae can be obtained by choosing appropriate values for $\zeta$ and $\eta$. Introducing Equation (2) into Equation (4) gives:

$$\left\{1 - \sigma_1\left[\left(\frac{\partial F_1^k}{\partial u}\right)_x + \left(\frac{\partial G_1^k}{\partial u}\right)_{xx} + \left(\frac{\partial F_2^k}{\partial u}\right)_y + \left(\frac{\partial G_2^k}{\partial u}\right)_{yy}\right]\right\}(\Delta u^k)$$

$$= \sigma_3 \Delta u^{k-1} + \sigma_2[(F_1^k)_x + (G_1^k)_{xx} + (F_2^k)_y + (G_2^k)_{yy} + (H^k)_{xy}]$$

$$+ \sigma_1\left[\left(\frac{\partial F_1^k}{\partial h}\Delta h^k\right)_x + \left(\frac{\partial G_1^k}{\partial h}\Delta h^k\right)_{xx} + \left(\frac{\partial F_2^k}{\partial h}\Delta h^k\right)_y + \left(\frac{\partial G_2^k}{\partial h}\Delta h^k\right)_{yy} + (\Delta H^{k-1})_{xy}\right], \quad (6)$$

where the subscripts $x$ and $y$ refer to partial differentiation with respect to those independent variables. The bracketed quantity on the left-hand-side of Equation (6) denotes a linear, differential operator that operates on $\Delta u^k$. Upon factorization, the following one-dimensional equations are obtained:

$$\Delta u^* + \left[-\sigma_1 \frac{\partial F_1^k}{\partial u}\Delta u^*\right]_x + \left[-\sigma_1 \frac{\partial G_1^k}{\partial u}\Delta u^*\right]_{xx} = V_x^k + W_{xx}^k + Z^{k,k-1} \quad (7)$$

and

$$\Delta u^k + \left[-\sigma_1 \frac{\partial F_2^k}{\partial u}\Delta u^k\right]_y + \left[-\sigma_1 \frac{\partial G_2^k}{\partial u}\Delta u^k\right]_{yy} = \Delta u^*, \quad (8)$$

where $\Delta u^*$ is a dummy variable, and the additional functions $V^k$, $W^k$, $Z^{k,k-1}$ are defined as follows:

$$V^k = \sigma_2 F_1^k + \sigma_1 \frac{\partial F_1^k}{\partial h}\Delta h^k, \quad (9)$$

$$W^k = \sigma_2 G_1^k + \sigma_1 \frac{\partial G_1^k}{\partial h}\Delta h^k, \quad (10)$$

$$Z^{k,k-1} = \sigma_2[(F_2^k)_y + (G_2^k)_{yy} + (H^k)_{xy}] + \sigma_1\left[\left(\frac{\partial F_2^k}{\partial h}\Delta h^k\right)_y + \left(\frac{\partial G_2^k}{\partial h}\Delta h^k\right)_{yy} + (\Delta H^{k-1})_{xy}\right]$$

$$+ \sigma_3 \Delta u^{k-1}. \quad (11)$$

The solution is accomplished in two stages. The intermediate values $(\Delta u^*)$ are first computed from Equation (7) by sweeping in the $x$-direction. Then, the intermediate results are used on the right-hand-side of Equation (8) to generate the values of the unknowns at the new time level by sweeping in the $y$-direction.

If $u(x, y, t)$ and $h(x, y, t)$ are vectors, then all derivatives with respect to $u$ and $h$ in Equations (7)–(11) are replaced with the corresponding Jacobians.

## 2.2. Discretization of the computational domain

For a problem with boundary or interior layers, it is often preferable to subdivide the computational domain into two (or more) subdomains of different grid resolutions in order to refine only those regions where large gradients are encountered. The uniform grid spacing, $\Delta x_0$, is defined as:

$$\Delta x_0 = L/(nx - 1), \tag{12}$$

where $L$ is the length of the domain and $nx$ is the initial number of grid points. Next, as shown in Figure 1, the last $k_n$ uniform spacings are replaced with a subdomain refined geometrically with a progression ratio $r > 1$ according to the relation:

$$\Delta x_i = r\Delta x_{i-1}, \quad \text{for } i = 2, \ nr - 1, \tag{13}$$

where $nr$ is the number of grid points in the non-uniform subdomain. As a result of domain decomposition, the total number of grid points in the computational domain becomes:

$$nt = nx - k_n + nr. \tag{14}$$

The first non-uniform spacing is taken to be a fraction $r_0$ of the uniform grid spacing $\Delta x_0$, i.e.

$$\Delta x_1 = r_0 \Delta x_0. \tag{15}$$

The value of $r$ is given implicitly by the relation:

$$k_n = r_0 \frac{(r^{nr-1} - 1)}{r - 1}. \tag{16}$$

The grid points are distributed in the non-uniform subdomain so that the last spacing is smaller than a corrected boundary layer thickness, namely:

$$\Delta x_{nr-1} \leq \varepsilon/k_a, \tag{17}$$

where $k_a$ is an 'assurance factor' used to guarantee the placement of at least a few grid points in the thin layer, and $\varepsilon$ is the estimated thickness of the boundary layer.

The parameters $\Delta x_0$, $k_a$, $k_n$ and $r_0$ control the grid distribution in the computational domain. Hence, it is important to ascertain their influence if an appropriate grid is to be prescribed. By combining Equations (16) and (17), one can obtain a relation for the non-uniform grid ratio $r$ in terms of the four control parameters:

$$r = \frac{k_n - r_0}{k_n - \varepsilon/(k_a \Delta x_0)}. \tag{18}$$

For a typical stiff problem (i.e. $\varepsilon \ll 1$), $r$ depends very weakly on $\Delta x_0$ or $k_a$. The two parameters $\Delta x_0$ and $k_a$ exert a fine control on the geometric progression ratio $r$, while $k_n$ and $r_0$ exert a
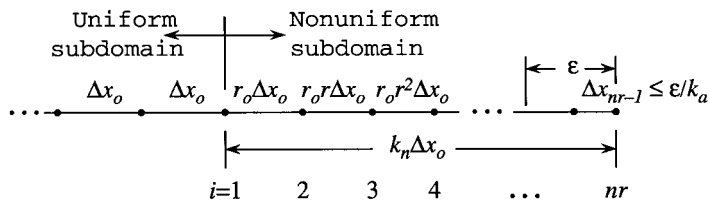


Figure 1. Interface grid distribution with grid parameters $\Delta x_0$, $k_n$, $k_a$ and $r_0$ defined.

rough control on the value of $r$. The parameter $k_n$ being an integer provides a discrete control over the ratio $r$, while $r_0$, which is a real number, exerts a continuous control over $r$.

## 2.3. Spatial approximation in a non-uniform mesh

The two fourth-order-accurate FD schemes employed in this paper are the pentadiagonal and tridiagonal [14] schemes, and are referred to here as classical and compact [18] respectively. When approximating a spatial derivative in a given direction at a grid point, compact FD approximations present the advantage of involving less neighbors than classical fourth-order methods (three instead of five in each spatial direction).

However, the compact FD schemes are tedious to derive for non-uniform grid distributions by use of Taylor series expansions. Hence, in a geometrically refined grid, numerical differentiation by means of Chebyshev polynomials [12] or spline interpolation [17] provide a more systematic approach to deriving high-order approximation formulae. As an example, the fourth-order compact FD approximation will be derived by means of Legendre interpolation. The approximations of the first and second derivatives, given by 5-point Legendre interpolation on a non-uniform mesh [20] are:

$$f'(x_j) = \sum_{k=1}^{5} f(x_k)L_k'(x_j) \quad \text{and} \quad f''(x_j) + \sum_{k=1}^{5} f(x_k)L_k''(x_j), \tag{19}$$

where $L_k(x)$ is the $k$th Legendre polynomial (see Appendix A for details). The centered compact FD approximations for the first and second derivatives appear as:

$$\left.\begin{array}{l} \alpha_1 f'(x_{j-1}) + f'(x_j) + \beta_1 f'(x_{j+1}) = [\rho_1 f(x_{j-1}) + \xi_1 f(x_j) + \tau_1 f(x_{j+1})]/\Delta x_j, \\ \text{and} \\ \alpha_2 f''(x_{j-1}) + f''(x_j) + \beta_2 f''(x_{j+1}) = [\rho_2 f(x_{j-1}) + \xi_2 f(x_j) + \tau_2 f(x_{j+1})]/\Delta x_j^2. \end{array}\right\} \tag{20}$$

respectively, where the former is fourth-order-accurate and the latter is third-order-accurate.

The compact discretization of Equations (7) and (8) is illustrated on the following equation:

$$f + (Af)_x + (Bf)_{xx} = Z + W_x + V_{xx}, \tag{21}$$

where $A$, $B$, $Z$, $W$ and $V$ are functions identified by comparing Equation (21) with each of the original Equations (7) and (8). Formulae (20) can be written, in shorthand notation, as:

$$\left.\begin{array}{l} \mathcal{F}(f') = \mathcal{G}(f), \\ \text{and} \\ \mathcal{S}(f'') = \mathcal{T}(f), \end{array}\right\} \tag{22}$$

where $\mathcal{F}$, $\mathcal{G}$, $\mathcal{S}$ and $\mathcal{T}$ are linear operators.

By applying formulae (22) on Equation (21), one obtains the following final form of the finite difference equation:

$$\mathcal{F}(\mathcal{S}(f)) + \mathcal{S}(\mathcal{G}(Af)) + \mathcal{F}(\mathcal{T}(Bf)) = \mathcal{F}(\mathcal{S}(Z)) + \mathcal{S}(\mathcal{G}(W)) + \mathcal{F}(\mathcal{T}(V)). \tag{23}$$

With this approach, the one-sided formulae near the boundaries and interfaces can be obtained as conveniently as the centered FD formulae. Although the following discussion on FD discretization at grid boundaries is concerned with problems that are subject to Dirichlet boundary conditions, the methodology presented here is not limited to these types of problems. At grid points adjacent to boundaries, one-sided approximations are derived for the compact

operators [14], in which a 2-point stencil for the operators $\mathscr{F}$ and $\mathscr{S}$ (identical in this case) was used, and one-sided, 5-point stencil operators for $\mathscr{G}$ and $\mathscr{T}$. As a result, the following finite difference equation is obtained at the boundaries:

$$\mathscr{F}(f) + \mathscr{G}(Af) + \mathscr{T}(Bf) = \mathscr{F}(Z) + \mathscr{G}(V) + \mathscr{T}(W). \tag{24}$$

In order to better understand the FD discretization used at the boundaries, the finite difference equations used near grid boundaries are presented next. For the sake of simplicity in the following discussion, it is understood that the grid distribution adjacent to the left boundary is uniform while that near the right boundary is non-uniform. Hence, the uniform grid FD formulae used for the first and second derivatives near the left boundary become:

$$f'(x_1) + 10f'(x_2) = \frac{-55f(x_1) - 52f(x_2) + 144f(x_3) - 44f(x_4) + 7f(x_5)}{12\Delta x}, \tag{25}$$

$$f''(x_1) + 10f''(x_2) = \frac{145f(x_1) - 304f(x_2) + 174f(x_3) - 16f(x_4) + 7f(x_5)}{12\Delta x^2}. \tag{26}$$

At the right boundary, where the grid distribution is considered to be non-uniform, the derivatives are approximated by the use of Legendre interpolation polynomials at location $x = x_{nt-1}$ by the use of the one-sided, 5-point grid stencil $(nt-4, nt-3, nt-2, nt-1, nt)$:

$$f'(x_{nt-1}) = \sum_{k=nt-4}^{nt} f(x_k)L'_k(x_{nt-1}) \quad \text{and} \quad f''(x_{nt-1}) = \sum_{k=nt-4}^{nt} f(x_k)L''_k(x_{nt-1}), \tag{27}$$

where $L_k(x)$ is the $k$th Legendre polynomial (see Appendix A).

Additionally, the use of Legendre interpolation provides a straightforward approach to deriving fourth-order FD formulae at the interface between subdomains where different growth ratios are used in refining the grid. At the interface between the uniform and non-uniform grids, where two ratios $r_0$ and $r$ are used to discretize the grid, the formal compact differentiation given by the relation (23) is not valid. The compact differentiation does not hold because the left-hand-side FD operators, $\mathscr{F}$ for the first derivative and $\mathscr{S}$ for the second derivative respectively, are not identical for the neighboring points. For the neighboring grid points around the interface between the uniform and non-uniform grids the same 5-point central, classical FD formulas are used for both compact and classical FD approximations.


## 3. TEST PROBLEMS

Two different representative equations whose solutions exhibit boundary or interior layers are used in this investigation. For the case of the Burgers equation, both the shock and the sine wave problems are studied. For the case of the Reynolds equation of lubrication, the problem of an air bearing separating a smooth translating surface and a sinusoidally textured stationary slider is considered [21].

### 3.1. Burgers equation

The simplest equation combining non-linear convection and diffusion effects is the Burgers equation, which when written in conservation form appears as:

$$\frac{\partial u}{\partial t} = \frac{\partial}{\partial x}(\alpha u - 0.5u^2) + \frac{\partial^2}{\partial x^2}(vu), \tag{28}$$

where $v$ is the kinematic viscosity and $\alpha$ is a constant. For the sine wave propagating problem, $\alpha = 0$ and the initial and boundary conditions are:

$$u(x, 0) = -\sin(\pi x), \qquad u(-1, t) = u(0, t) = 0. \tag{29}$$

For small values of $v$, the solution develops into a sawtooth wave at the origin. The exact solution is obtained by Hermite integration of the solution provided by the Cole–Hopf transformation.

A second Burgers problem, that of a stationary shock wave, is also considered by setting $\alpha = 0.5$, along with the following initial and boundary conditions:

$$u(-2, t) = 1, \qquad u(0, t) = 0, \qquad u(x, 0) = \begin{cases} 1 & \text{if } x < 0 \\ 0.5 & \text{if } x = 0 \\ 0 & \text{if } x > 0 \end{cases}. \tag{30}$$

Initially, the solution is a shock located at $x = 0$. As time progresses, the stationary shock is smoothed by the dissipative term. Since Hermite integration applied to compute the integrals involved in the Cole–Hopf solution does not provide accurate exact solutions for this Burgers problem with $v \leq 10^{-3}$, the exact solution is written in an alternative form [22]:

$$u_{ex}(x, t) = \cfrac{1}{1 + \exp[(x - 0.5t)/(2v)] \, \dfrac{\text{erfc}[-x/\sqrt{4vt}]}{\text{erfc}[(x - t)/\sqrt{4vt}]}}. \tag{31}$$

## 3.2. Reynolds equation of lubrication

The Reynolds equation of lubrication is considered because of its non-linear nature and because for an inclined, plane, infinitely wide, slider bearing, it has an exact solution that was provided by Burgdorfer [23]. In this work, however, the more general case of a finite width bearing is considered. In non-dimensional conservative form, the compressible two-dimensional Reynolds equation [2] appears as:

$$\frac{\partial u}{\partial t} = \frac{\partial}{\partial x}(u + 1.5u^2 h_x/\Lambda) + \frac{\partial^2}{\partial x^2}(0.5u^2 h/\Lambda) + R^2 \frac{\partial}{\partial y}(1.5u^2 h_y/\Lambda) + R^2 \frac{\partial^2}{\partial y^2}(0.5R^2 u^2 h/\Lambda), \tag{32}$$

where $u = ph$, $p(x, y, t)$ is the fluid pressure, $h(x, y, t)$ is the bearing clearance, $R$ is the bearing length to width aspect ratio, and $\Lambda = 6\mu V L_x/(P_a H_0^2)$ is the gas bearing number. Here, $\mu$ is the fluid viscosity, $V$ is the velocity of the translating surface, $L_x$ is the slider length, $P_a$ is the ambient pressure, and $H_0$ is the clearance at the trailing edge of the slider. For a finite width wedge gas bearing in which only the stationary slider is sinusoidally textured, the clearance height function $h$ is given by:

$$h(x, y, t) = h_1 + (1 - h_1)x + \varepsilon \sin(\beta x), \tag{33}$$

where $h_1$ is the inlet to outlet clearance ratio, $\varepsilon$ is the roughness amplitude, and $\beta$ is the roughness angular frequency. Equation (32) is solved subject to initial and boundary conditions of an ambient pressure. The pressure solutions exhibit side and trailing edge boundary layers whose thicknesses are of order $\Lambda^{-1/2}$ and $\Lambda^{-1}$ respectively. The bearing number $\Lambda$ can vary over a wide range from 1 to $10^7$ (see e.g. [10]).
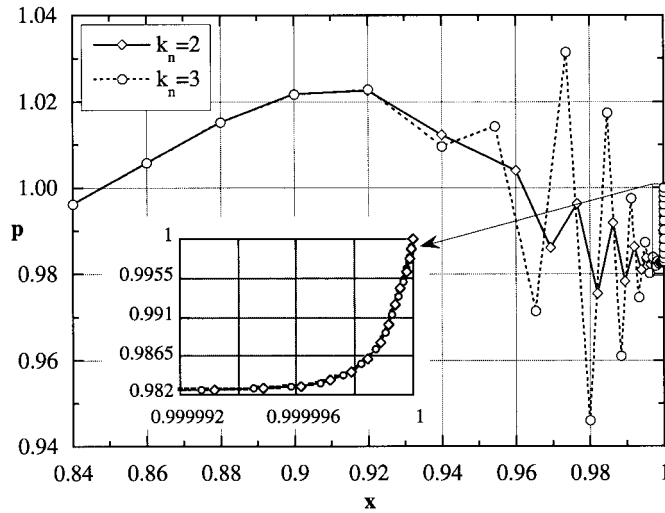
Figure 2. Pressure solution for a textured slider bearing after five time steps for a boundary layer thickness equal to $10^{-6}$, $\Delta x_0 = 0.02$ and $k_a = 15$.

## 4. INTERFACE SENSITIVITY

It is widely known that when solving problems with internal or boundary layers, numerical oscillations can appear in and around the layers if these are not adequately resolved with appropriately high spatial resolutions. For the test problems considered in this work, the authors have discovered, however, that numerically generated oscillations appear at the interface between the uniform and the non-uniform grid subdomains *even when* the boundary or interior layers are properly resolved. These oscillations will be referred to as interface oscillations. The authors quickly point out, however, that even though the oscillations appear at the interface, the interface is not the source of these oscillations. As will be shown in this section, the oscillations are due to an inappropriate value of the grid ratio used to geometrically distribute grid points in the non-uniform subdomain. These interface oscillations are observed in solutions obtained both with classical and compact schemes. In the remainder of this section, some of the basic features of the interface oscillations are analyzed and the role played by the interface grid distribution in eliminating them is investigated.

First, it is established that the interface oscillations do not result from an inappropriate resolution of the boundary layer. The pressure solutions in Figure 2 exhibit spurious oscillations even though the boundary layer is adequately resolved. Indeed, placing more grid points in the boundary layer by increasing $k_a$ has little effect on the interface oscillations as can be seen in Figure 3. Therefore, the oscillations do not originate from the boundary layer. We find, in fact, that the oscillations appear around the interface between the uniform and non-uniform grid subdomains. As the interface is moved by varying $k_n$, the oscillations are seen to move accordingly, as shown in Figure 2.

Second, the effects of the uniform grid spacing $\Delta x_0$ on the interface oscillations are examined and it is noted that only small reductions in their intensity are achieved as $\Delta x_0$ is decreased. For example, when the Reynolds problem is solved with the compact scheme for a bearing number $\Lambda = 10^6$ and a grid distribution generated with $k_n = 3$, $k_a = 15$ and $r_0 = 1$, strong oscillations appear after a few time steps and the solution shortly thereafter blows up even as
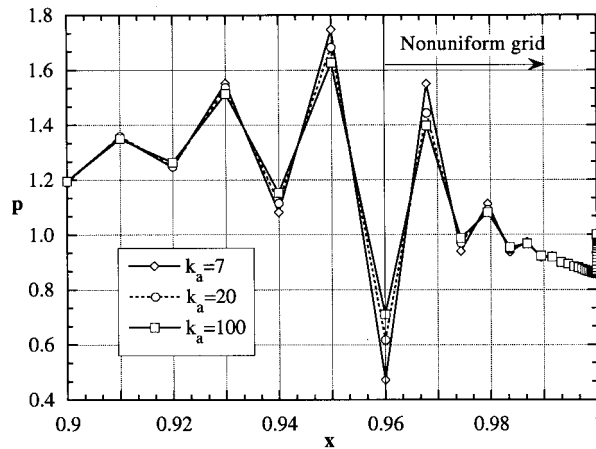
Figure 3. Pressure solutions after ten time steps with a boundary layer thickness equal to $10^{-6}$ and with grid parameters $\Delta x_0 = 10^{-2}$, $r_0 = 0.8$ and $k_n = 4$.

$\Delta x_0$ is varied from 0.01 to 0.002. A further reduction of $\Delta x_0$ from 0.00167 to 0.00083 reduces the maximum amplitude of the oscillations from 0.065 to 0.0058, but does not eliminate the oscillations, although the total number of grid points $nt$ is increased from 634 to 1232. The results of another example that involves the solution of the Burgers shock wave problem are summarized in Table I for two different but equivalent grid configurations. For either case, as the number of grid points increases from 177 to 1739, the geometric progression ratio $r$ remains nearly constant as indicated by Equation (18), and the root-mean-square (rms) errors decrease by only a factor of 3. The *rms error* values shown are a measure of the discrepancy between the numerical and exact results. Therefore, it is not satisfactory to refine the entire grid by reducing the uniform spacing $\Delta x_0$ in order to eliminate the interface oscillations.

Third, it is established that interface oscillations are mitigated by varying $r_0$. As shown in Figure 4 for the sinusoidally textured slider problem, the interface oscillations become apparent after only ten time steps, and if the solution is continued, these oscillations would spread out over the entire domain and even lead to divergence for cases with $r_0 > 0.75$. However, if $r_0$ is reduced from 0.75 to 0.65, the oscillations decrease in intensity and are finally eliminated when $r_0 = 0.65$, as shown in Figure 5. Furthermore, contrary to the case when $\Delta x_0$ was reduced, variations in $r_0$ do not dramatically increase the total number of grid points $nt$. For example, reducing $r_0$ from 0.8 to 0.72 increases the total number of grid points from 152 to only 158, while the maximum amplitude of the oscillations drops considerably from 0.56 to

Table I. The effect of $k_n$ and $r_0$ on the grid distribution and the rms error at $t = 0.2$ for the Burgers shock wave problem with $Re = 10^6$ and $\Delta t = 0.005$

| $\Delta x_0$ | $k_n = 6$; $r_0 = 1.0$; $k_a = 15$ | | | $k_n = 4$; $r_0 = 0.7143$; $k_a = 15$ | | |
|---|---|---|---|---|---|---|
| | $nt$ | $r$ | rms error | $nt$ | $r$ | rms error |
| 0.01 | 177 | 0.8571432 | 9.06886E−4 | 177 | 0.8571405 | 9.07108E−4 |
| 0.001848 | 606 | 0.8571450 | 4.88110E−4 | 606 | 0.8571429 | 4.88221E−4 |
| 0.000979 | 1082 | 0.8571468 | 3.65069E−4 | 1082 | 0.8571454 | 3.65150E−4 |
| 0.000594 | 1739 | 0.8571492 | 2.87932E−4 | 1739 | 0.8571486 | 2.87994E−4 |
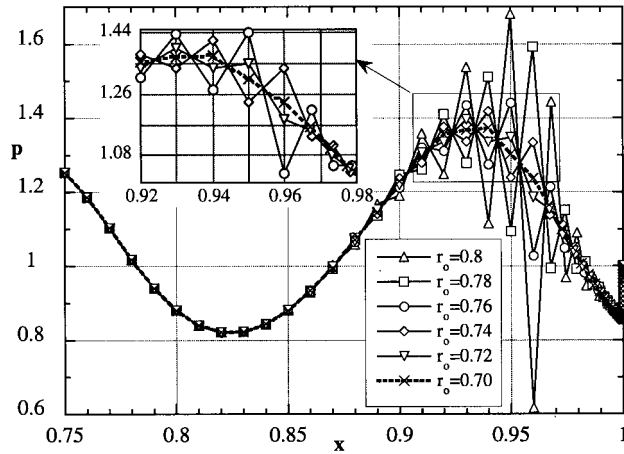
Figure 4. Pressure solutions after ten time steps with a boundary layer thickness equal to $10^{-6}$ and with grid parameters $\Delta x_0 = 10^{-2}$, $k_n = 2$ and $k_a = 15$.

0.08. Consequently, given a $k_n$, there exists a range of $r_0$ for which the oscillations are reduced and eventually eliminated. An optimum upper bound value for $r_0$ can be identified by slowly decreasing it, in steps of 0.01, until convergence is attained and an accurate solution is obtained. For example, considering the compact scheme and a grid distribution given by $\Delta x_0 = 0.01$, $k_n = 2$ and $k_a = 15$, the optimum $r_0$ value is found to be 0.51 as shown in Table II. When the analysis is repeated for the Burgers equation, the same behaviors are observed for both the boundary layer and the interior layer problems. For example, in Figure 6 the interface oscillations are seen to decay for solutions of the Burgers sine wave problem as $r_0$ is reduced.

Last, it is established that interface oscillations can also be mitigated by varying $k_n$ since $r_0$ and $k_n$ are shown to play complementary roles. The influence of $k_n$ on the oscillations is investigated because a smaller $k_n$ value implies a shorter non-uniform subdomain, which should, at first glance, lead one to the conclusion that a given problem can be solved with less
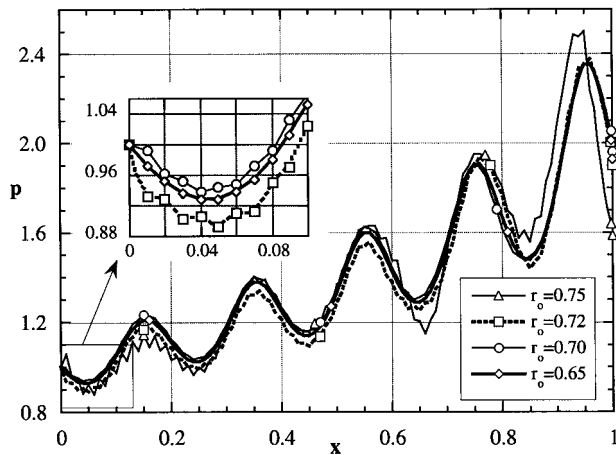


Figure 5. Steady state pressure solutions with a boundary layer thickness equal to $10^{-6}$ and with grid parameters $\Delta x_0 = 10^{-2}$, $k_n = 2$ and $k_a = 15$.

Table II. Convergence of the Reynolds solution as $r_0$ is decreased with $\Lambda = 10^{-6}$, $\Delta x_0 = 0.01$, $k_n = 4$, $k_a = 15$ and $\Delta t = 0.005$

| $r_0$ | $r$ | $nt$ | rms ($\Delta u^n$) | Comments |
|---|---|---|---|---|
| 0.54 | 0.8200014802 | 157 | 3.82917E−03 | Large oscillations |
| 0.53 | 0.8233345844 | 159 | 2.92099E−04 | Large oscillations |
| 0.52 | 0.8266682373 | 159 | 5.96837E−06 | Small oscillations |
| 0.51 | 0.8300013564 | 161 | 4.47539E−06 | Accurate solution |
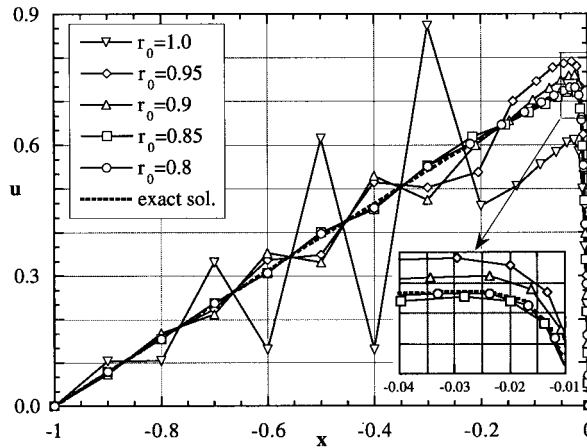


Figure 6. Burgers sine wave solution at $t = 3\pi$ for $v = 1/(100\pi)$ and $\Delta t = 1/(200\pi)$ and with grid parameters $\Delta x_0 = 0.1$, $k_n = 3$ and $k_a = 5$.

grid points. It was previously noted with reference to Table II that corresponding to the optimal value of $r_0$, a threshold value of $r$ (and hence of $nt$) is achieved. Indeed, for a chosen FD scheme and each given value of $\Delta x_0$, there exist threshold values for $r$ and $nt$ that correspond to the optimal values of $r_0$, and are independent of $k_n$. Let the threshold values be denoted by $r^*$ and $nt^*$. As an example, the parameters $r^*$ and $nt^*$ for two values of $k_n$ and the corresponding values of $r_0$ are summarized in Table III for solutions of the Reynolds and Burgers problems. The threshold values of $r^*$ and $nt^*$ were determined for each case by the same procedure described with reference to the results of Table II. Examination of Table III indicates that as $k_n$ is doubled from 2 to 4, the values of $r^*$ and $nt^*$ experience insignificant changes. Therefore, the total number of grid points for which the oscillations are eliminated

Table III. Threshold growth factor $r^*$ and total number of grid points $nt^*$ for the Reynolds problem with $\Lambda = 10^6$, $k_a = 15$, $\Delta t = 0.005$ and $\Delta x_0 = 10^{-2}$; and the Burgers problem with $v = 1/(100\pi)$, $k_a = 4$, $\Delta t = 1/(200\pi)$ and $\Delta x_0 = 0.1$

| Non-uniform grid parameters | Reynolds problem | | | | Burgers problem | | | |
|---|---|---|---|---|---|---|---|---|
| | Classical | | Compact | | Classical | | Compact | |
| $k_n$ | 2 | 4 | 2 | 4 | 1 | 2 | 1 | 2 |
| $r_0$ | 0.45 | 0.75 | 0.50 | 0.85 | 0.50 | 0.75 | 0.50 | 0.80 |
| $r^*$ | 0.850 | 0.850 | 0.833 | 0.830 | 0.753 | 0.752 | 0.735 | 0.735 |
| $nt^*$ | 168 | 169 | 161 | 161 | 25 | 25 | 25 | 24 |

($nt^*$) is the same, irrespective of $k_n$. This outcome is anticipated from the previous examination of Table I, where it was observed that two different pairs of $k_n$ and $r_0$ have yielded identically accurate solutions with nearly identical values of $nt$, $r$ and *rms error*. The same complementary behavior of $k_n$ and $r_0$ is observed in the solutions of the Burgers equation, the results of which are also summarized in Table III.

The aforementioned effects on the interface oscillations by the grid distribution parameters $k_a \Delta x_0$, $r_0$ and $k_n$ can be interpreted by considering their influence on the resultant geometric ratio $r$ within the non-uniform subdomain. For each scheme and each value of $\Delta x_0$ considered, a range of the geometric ratio exists in which the oscillations are reduced until they are completely eliminated (provided of course that the boundary layer is resolved by a proper value of $k_a$). However, large variations in $k_a$, which attenuate the oscillations, are not sufficient to bring $r$ into the range where the oscillations are completely eliminated. On the other hand, small variations in either $k_n$ or $r_0$ bring the value of $r$ into the range where oscillations are promptly mitigated. These observations are supported by the conclusions of Section 2.2, where it was shown that the geometric factor $r$ is weakly dependent on $k_a$ and $\Delta x_0$ and strongly dependent on $k_n$ and $r_0$.

Finally, interface oscillations in two-dimensional boundary layer problems are investigated by examining solutions of the two-dimensional Reynolds equation of lubrication. The same behavior with regard to interface oscillations observed in the one-dimensional cases is observed in their two-dimensional counterparts. For example, in Figure 7, the oscillations are seen to decrease as the value of $r_{0x}$ is lowered from 0.57 to 0.53. A closer view of the effect of $r_{0x}$ on the interface oscillations in the $x$-direction is shown in Figure 8, where the pressure at the grid point ($x = 0.15$, $y = 0.5$) is plotted versus $r_{0x}$ with all other grid parameters held fixed. The value of the pressure is seen to converge as $r_{0x}$ approaches a value of 0.5, which is identical to the threshold value encountered in the one-dimensional case. Therefore, the two-dimensional interface oscillations generated by the fourth-order FD schemes can be controlled by the grid control parameters in the same manner as in the one-dimensional case.

## 5. RELATION TO MESH REYNOLDS NUMBER

In the previous sections, it was demonstrated that the observed oscillations at the interface of two subdomains, one with a uniform and the other with a non-uniform grid distribution, are due to an inappropriate distribution of grid points in the non-uniform subdomain. It was further determined that these numerical oscillations were present in the solutions obtained by the use of both compact and classical FD schemes, including the popular second-order FD scheme. While a non-linear stability analysis is not possible, the theory of linear stability can be used to predict a mesh Reynolds number threshold value of 2 for the second-order discretization. The aim of this final section is to investigate whether a connection exists between the mesh Reynolds number and the occurrence of interface oscillations.

The results of solving the Burgers sine wave problem with a centered, second-order FD scheme are shown in Figure 9 for different values of the interface grid ratio $r_0$. Along with the FD solutions, the exact solution is shown for comparison. It can be observed that the interface oscillations decrease in magnitude and finally disappear as $r_0$ is reduced. An enlargement of the steep region near $x = 0$ is given in Figure 10 to better highlight this behavior. The results for $r_0 = 0.6$ track the exact solution rather closely, providing confidence that the FD solution has converged and is free of spurious interface oscillations. The local mesh Reynolds number is plotted for the four $r_0$ cases considered in Figure 11. The results indicate that the presence and
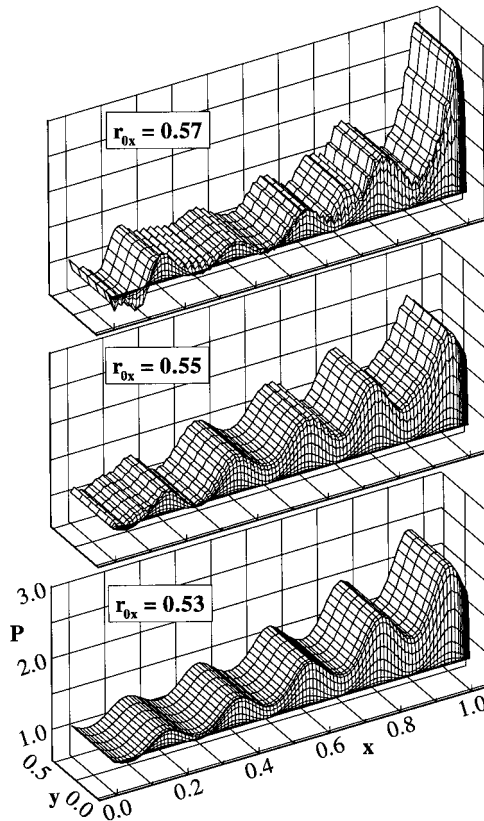
Figure 7. Two-dimensional steady state pressure solutions for the Reynolds equation with a trailing edge boundary layer thickness equal to $10^{-6}$ and with grid parameters $r_0 = 0$ 57, 0.55 and 0.53; $\Delta x_0 = 10^{-2}$; $k_n = 3$; and $k_a = 15$.
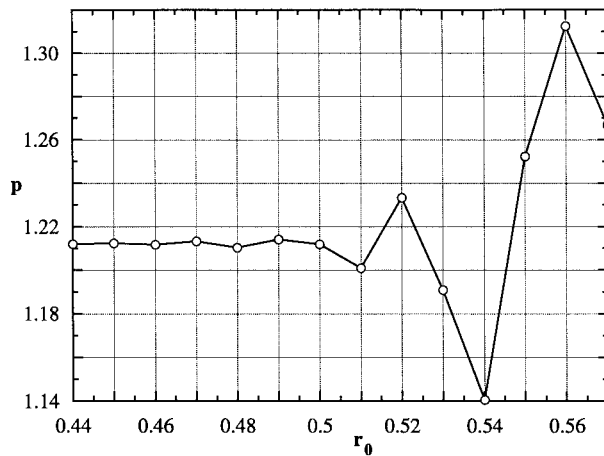


Figure 8. Pressure solution at the point ($x = 0.15$, $y = 0.5$) for the two-dimensional Reynolds equation with $\Lambda = 10^{-6}$ and with grid parameters $\Delta x_0 = 10^{-2}$, $k_n = 2$ and $k_a = 15$.
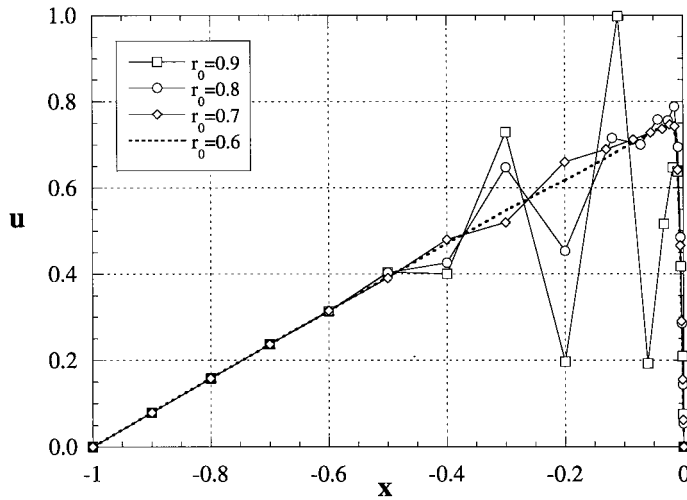
Figure 9. Burgers sine wave solution for $v = 10^{-2}/\pi$ at $t = 3/\pi$ using second-order FD ($\Delta t = 1/(200\pi)$, $\Delta x_0 = 0.1$, $k_n = 2$, $k_a = 4$).

disappearance of the oscillations are unrelated to the mesh Reynolds number since not only does the latter remain well above the threshold value of 2 (predicted by the theory of linear stability) for most of the computational domain, but it does not change appreciably around the interface, where the oscillations are present at higher values of $r_0$.

## 6. CONCLUSIONS

Solutions of the non-linear Burgers and Reynolds equations, which possess sharp interior and boundary layers, have been used to investigate the mitigation and elimination of scheme-related spurious oscillations of fourth-order FD schemes. The effects of the grid control
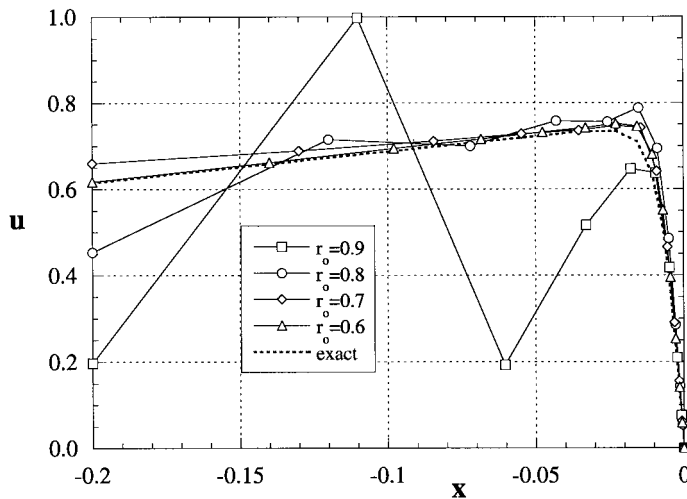


Figure 10. Enlargement of boundary layer region in Figure 9.
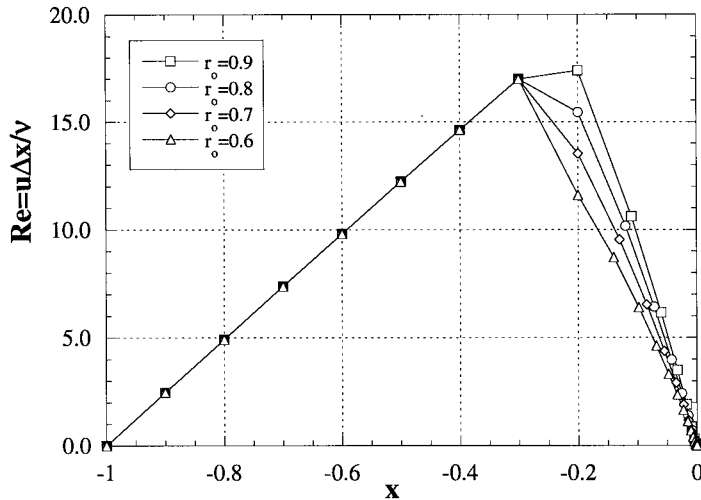
Figure 11. Local mesh Reynolds number for Burgers sine wave problem with $v = 10^{-2}/\pi$ at $t = 3/\pi$ using second-order FD scheme ($\Delta t = 1/(200\pi)$, $\Delta x_0 = 0.1$, $k_n = 2$, $k_a = 4$).

parameters on the grid distribution within the non-uniform subdomains have been ascertained in order to enable the prescription of an optimal grid distribution that resolves the boundary and interior layers while avoiding the appearance of spurious oscillations.

For both the Reynolds and Burgers problems, numerical oscillations are observed to appear around the interface between the uniform and the non-uniform grid subdomains. It is demonstrated, however, that the interface is not the source of these oscillations. Rather, the oscillations are due to low values of the grid progression ratio used to discretize the non-uniform subdomains. In fact, it is indicated that for each scheme there is a threshold grid ratio above which the numerical oscillations are eliminated. As conjectured in the literature, ratios used to distribute grid points non-uniformly should remain close to 1 in order to maintain the higher formal accuracy of finite difference approximations for uniform grids. Indeed, it is observed in this work that as the grid ratios are increased well above the threshold ratios, the solutions continue to improve.

This work demonstrates that high-order classical and compact schemes can be used with confidence to efficiently solve one- or two-dimensional problems that possess stiff layers, provided that scheme-related oscillations are eliminated by a proper choice of the grid parameters $k_n$ and $r_0$.

## APPENDIX A. LEGENDRE POLYNOMIALS

On a local grid distribution $(x)_{i=1,m}$, the $k$th Legendre interpolating polynomial of order $m$ and its derivatives at a location $x$ are:

$$L_k(x) = \prod_{\substack{i=1 \\ i \neq k}}^{m} \frac{(x - x_i)}{x_k - x_i}, \tag{34}$$

$$L_k'(x) = \sum_{l=1}^{m} \prod_{\substack{i=1 \\ i \neq k,l}}^{m} \frac{(x - x_i)}{x_k - x_i}, \tag{35}$$

$$L_k''(x) = \sum_{l=1}^{m} \sum_{n=1}^{m} \prod_{\substack{i=1 \\ i \neq k,l,n}}^{m} \frac{(x-x_i)}{x_k - x_i}. \tag{36}$$

The fourth-order classical and compact FD approximations are derived using Legendre interpolating polynomials of order 5. As an example, the fourth-order compact formulae for a non-uniform mesh are presented. Using the relative increments with respect to the $j$th node $h_i = \Delta x_i / \Delta x_j$, the $k$th Legendre interpolating polynomial derivatives (35) and (36) can be written at the local nodes $x_i$ as functions of $(h)_{i=1,4}$, $\Delta x_j$ and $\Delta x_j^2$ in the following forms:

$$L_k'(x_i) = T_{ki}(h_1, h_2, h_3, h_4)/\Delta x_j, \tag{37}$$

$$L_k''(x_i) = S_{ki}(h_1, h_2, h_3, h_4)/\Delta x_j^2. \tag{38}$$

If the expression $\alpha_1 f'(x_{j-1}) + f'(x_j) + \beta_1 f'(x_{j+1})$ is expanded by the use of the Legendre interpolation for the first derivatives $f'(x_{j-1})$, $f'(x_j)$ and $f''(x_{j+1})$ given by Equations (19) and (37), and the contributions from the end points are canceled out, the constants $\alpha_1$ and $\beta_1$ can be determined from the solutions of the following two algebraic relations:

$$\begin{cases} \alpha_1 T_{12} + \beta_1 T_{14} = -T_{13} \\ \alpha_1 T_{52} + \beta_1 T_{54} = -T_{53} \end{cases}. \tag{39}$$

The fourth-order compact FD scheme for the first derivative is then given by:

$$\alpha_1 f'(x_{j-1}) + f'(x_j) + \beta_1 f'(x_{j+1}) = (\rho_1 f(x_{j-1}) + \xi_1 f(x_j) + \tau_1 f(x_{j+1}))/\Delta x_j, \tag{40}$$

where the constants $\rho_1$, $\xi_1$ and $\tau_1$ are:

$$\begin{cases} \rho_1 = (\alpha_1 T_{22} + T_{23} + \beta_1 T_{24}), \\ \xi_1 = (\alpha_1 T_{32} + T_{33} + \beta_1 T_{34}), \\ \tau_1 = (\alpha_1 T_{42} + T_{43} + \beta_1 T_{44}). \end{cases} \tag{41}$$

The formulae provided by Rubin and Khosla [17] for a geometrically refined grid are hence obtained.

## REFERENCES

1. P.J. Roache, *Computational Fluid Dynamics*, Hermosa Publishers, Albuquerque, NM, 1972.
2. P.E. Raad and A. Karageorghis, 'A Chebyshev spectral collocation method for the solution of the Reynolds equation of lubrication', *J. Comput. Phys.*, **106**, 42–51 (1993).
3. C.A.J. Fletcher, *Computational Techniques for Fluid Dynamics*, Springer, New York, 1990.
4. I.M. Kuria and P.E. Raad, 'An implicit multidomain spectral collocation method for stiff highly non-linear fluid dynamics problems', *Comput. Methods Appl. Mech. Eng.*, **120**, 163–182 (1995).
5. I. Babuska, O.C. Zienkiewicz, J. Gago and E.R. Oliveira, *Accuracy Estimates and Adaptive Refinements in Finite Element Computations*, Wiley, New York, 1986.
6. P.R. Eiseman, 'Adaptive grid generation', *Comput. Methods Appl. Mech. Eng.*, **64**, 321–376 (1987).
7. P.M. Gresho and R.L. Lee, 'Don't suppress the wiggles they're telling you something', *Comput. Fluids*, **9**, 223–253 (1981).
8. B. Engquist, P. Lötsedt and B. Sjögreen, 'Non-linear filters for efficient shock computation', *Math. Comput.*, **52**, 509–537 (1989).
9. W. Shyy, M.-H. Chen, R. Mittal and H.S. Udaykumar, 'On the suppression of numerical oscillations using a non-linear filter', *J. Comput. Phys.*, **102**, 49–62 (1992).
10. A.N. Varghese and P.E. Raad, 'Surface texture effects on ultrathin finite width gas bearings', *ASME Adv. Inform. Storage Syst.*, **6**, 69–96 (1995).
11. B. Fornberg, 'Generation of finite difference formulas on arbitrarily spaced grids', *Math. Comput.*, **51**, 699–706 (1988).
12. P. Hoffman and K.C. Reddy, 'Numerical differentiation by high-order interpolation', *SIAM J. Sci. Stat. Comput.*, **8**, 979–987 (1987).

13. R.M. Beam and R.F. Warming, 'An implicit factored schemes for the compressible Navier–Stokes equation', *AIAA J.*, **16**, 393–402 (1978).
14. S.K. Lele, 'Compact finite difference schemes with spectral-like resolution', *J. Comput. Phys.*, **103**, 16–42 (1992).
15. E.C. Gartland, Jr., 'Compact high-order finite differences for interface problems in one dimension', *IMA J. Numer. Anal.*, **9**, 243–260 (1989).
16. Y. Adam, 'Highly accurate compact implicit methods and boundary conditions', *J. Comput. Phys.*, **24**, 10–22 (1977).
17. S.G. Rubin and P.K. Khosla, 'Polynomial interpolation methods for viscous flow calculations', *J. Comput. Phys.*, **24**, 217–244 (1977).
18. X. Aubert and M. Deville, 'Steady viscous flows by compact differences in boundary-fitted coordinates', *J. Comput. Phys.*, **49**, 490–522 (1983).
19. R.F. Warming and R.M. Beam, 'On the construction and application of implicit factored schemes for conservation law', *SIAM-AMS Proc.*, **11**, 85–129 (1978).
20. B. Carnahan, H.A. Luther and J.O. Wilkes, *Applied Numerical Methods*, Wiley, New York, 1969.
21. A. Cameron, *Basic Lubrication Theory*, Wiley, New York, 1976.
22. G.B. Whitham, *Linear and Non-linear Waves*, Wiley, New York, 1974.
23. A. Burgdorfer, 'The influence of the molecular mean free path on the performance of hydrodynamic gas lubricated bearings', *J. Basic Eng.*, **81**, 94–100 (1959).